J. Fluid Mech. (1996), *vol.* 315, *pp.* 65–84

Stability of a potential vorticity front: from quasi-geostrophy to shallow water

By E. BOSS[1], N. PALDOR[2] AND L. THOMPSON[1]

[1]School of Oceanography, University of Washington, Seattle, WA 98195-7940, USA

[2]Department of Atmospheric Sciences, The Hebrew University of Jerusalem, Jerusalem, Israel

(Received 12 October 1995 and in revised form 29 December 1995)

The linear stability of a simple two-layer shear flow with an upper-layer potential vorticity front overlying a quiescent lower layer is investigated as a function of Rossby number and layer depths. This flow configuration is a generalization of previously studied flows whose results we reinterpret by considering the possible resonant interaction between waves. We find that instabilities previously referred to as 'ageostrophic' are a direct extension of quasi-geostrophic instabilities.

Two types of instability are discussed: the classic long-wave quasi-geostrophic baroclinic instability arising from an interaction of two vortical waves, and an ageostrophic short-wave baroclinic instability arising from the interaction of a gravity wave and a vortical wave (vortical waves are defined as those that exist due to the presence of a gradient in potential vorticity, e.g. Rossby waves). Both instabilities are observed in oceanic fronts. The long-wave instability has length scale and growth rate similar to those found in the quasi-geostrophic limit, even when the Rossby number of the flow is $O(1)$.

We also demonstrate that in layered shallow-water models, as in continuously stratified quasi-geostrophic models, when a layer intersects the top or bottom boundaries, that layer can sustain vortical waves even though there is no apparent potential vorticity gradient. The potential vorticity gradient needed is provided at the top (or bottom) intersection point, which we interpret as a point that connects a finite layer with a layer of infinitesimal thickness, analogous to a temperature gradient on the boundary in a continuously stratified quasi-geostrophic model.

1. Introduction

Observations of frontal instabilities in the ocean (e.g. Watts & Johns 1982; Barth 1994) and laboratory experiments (Griffiths & Linden 1982; Griffiths, Killworth & Stern 1982) have motivated numerous studies of frontal instabilities within the framework of the shallow-water approximation (e.g. Killworth, Paldor & Stern 1984, hereafter referred to as KPS; Paldor & Ghil 1991).

In geophysical flows, fronts are identified as regions of rapid changes in the surface density or isopycnal depth. In the ocean, such density changes occur over horizontal distances of the order of the deformation radius, and are associated with jets and even more rapid changes in potential vorticity (PV) (Hall & Fofonoff 1993). We will argue below that a density front can be viewed as a PV front. While the quasi-geostrophic approximation (QG) is not strictly applicable for density fronts because of the $O(1)$ change in the depth of isopycnal surfaces and the $O(1)$ Rossby number of the flow

(in standard notation the Rossby number is $\epsilon \equiv U/Lf$, where U is the flow velocity, L its horizontal scale and f the Coriolis frequency), PV fronts can be modelled in this approximation (e.g. Pratt & Stern 1986). A question that arises, and that we will attempt to address here, is how the two approximations, namely QG and shallow water, compare in simulating PV fronts (or equivalently, density fronts) and their linear stability characteristics.

The simplest shallow-water model of a density front consist of a $1\frac{1}{2}$†- or 2-layer model in which the interface between the layers intersects the surface (an 'outcropping front'). In particular, KPS observed that an outcropping front in a 2-layer model, with a quiescent lower layer and constant PV in the upper layer, displays a long-wave instability with a similar length scale and growth rate to instabilities found in a QG model. Because there was no obvious PV front, they classified this instability as 'ageostrophic', i.e. involving dynamics not present in the QG approximation (see also Barth 1989, and Sakai 1988). We argue here that the instability observed in KPS (and others, such as Griffiths *et al.* 1982; Barth 1989; Swaters 1991) is quasi-geostrophic in nature, i.e. is the result of interaction of vortical waves. Vortical waves are defined as waves that exist due to the presence of a PV gradient (e.g. β-plane and topographic Rossby waves). These are the only waves present in the QG approximation.

Using Hayashi & Young's (1987) analysis of instabilities as resulting from resonant interactions of neutral waves, we show that the KPS instability is a result of the resonance of two vortical waves, and thus involves dynamics that are present in QG instabilities. However, since the upper layer has no PV gradient, a question arises as to how the fluid can sustain a vortical wave. In order to answer this question, we examine the upper and lower boundaries.

The role of the boundaries in QG instabilities is well established: for instance, in the Eady model the instability owes its existence to the temperature gradient imposed at the top and bottom boundaries. These boundaries are interpreted as δ-functions of PV (Bretherton 1966*a*). However, in shallow-water layered models of an outcropping front, the surface (or bottom) intersection point has not been recognized as a PV discontinuity. The free streamline of the outcropping front along which the upper layer vanishes can be regarded as the boundary between the upper layer and an infinitesimally thin layer of infinitely large PV. From the above argument it follows that in KPS's model, a vortical wave can exist in the vanishing upper layer which has constant PV, and the necessary PV gradient exists at the intersection point.

The richer dynamics found in the shallow-water approximation permit instabilities not found in the QG approximation, i.e. ageostrophic ones. These can arise, for example, from the interaction of waves that exist in QG models (vortical waves) with those not found in QG (such as gravity waves) as was shown by Sakai (1988) who found a Kelvin–Rossby wave instability. Here we demonstrate that a resonant interaction between a gravity wave and a vortical wave exists in the model investigated by KPS.

Important conserved quantities in the analysis of linear instabilities in inviscid flows are the pseudo-momentum and pseudo-energy (Hayashi & Young 1987). It was suggested by Sakai (1988) that the different terms of the pseudo-momentum each correspond to a different physical mode (vortical waves *vs.* gravity waves). One cannot use the frequency to differentiate between the modes as the gravity waves have Doppler-shifted frequencies similar to the vortical waves. Here, however, we show for

† A $1\frac{1}{2}$-layer model is a 2-layer model with either the upper or lower layer of infinite depth, also referred to as equivalent barotropic.

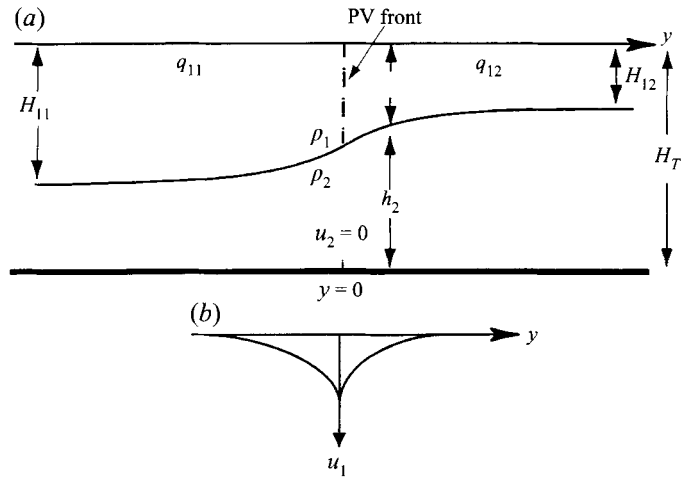

FIGURE 1. Schematics of the height (*a*) and velocity (*b*) fields of an upper-layer potential vorticity front. The upper-layer flow is geostrophic and has piecewise-constant PV, $q_{1j} = f/H_{1j}$, where j denotes the side of the front (1 being south, $y < 0$), the H_{1j} denote the depth of the upper-layer at $y \to \mp\infty$ respectively and the lower layer is quiescent. When $H_{12} = 0$, the interface between the layers intersects the surface, resulting in an outcropping front.

a simple case, first analysed by Williams (1991), that Sakai's conjecture fails, i.e. there is no one-to-one correspondence between the various terms in the pseudo-momentum and the physical modes. Instead, by varying the Rossby number of the flow and following the instability to its QG limit, we can differentiate between vortical modes and gravity wave modes.

The organization of the paper is as follows. Section 2 introduces the 2-layer shallow-water model which, by changing the Rossby number, spans configurations from a QG PV front to the outcropping front of KPS, and the linear stability problem is formulated. We then revisit previously published results from the $1\frac{1}{2}$-layer limit of the model in § 3. In § 4 these results are used to distinguish between different resonant interactions observed in the 2-layer model. In § 5, we apply the analogy of PV and density fronts to the barotropic case of Griffiths *et al.* (1982). We discuss our findings and conclude in § 6.

2. Formulation of the model

The problem we consider here is that of a surface geostrophic jet at the interface between two regions of constant PV but equal density ρ_1 (figure 1). The upper layer, where the jet resides, overrides a quiescent lower layer of density $\rho_2 > \rho_1$. We assume the fluid to be Boussinesq, hydrostatic, and to have a rigid lid on an f-plane, which we refer to as the shallow-water approximation. The momentum and continuity equations are

$$(\partial_t + \boldsymbol{u}_i \cdot \nabla)\boldsymbol{u}_i + f\hat{\boldsymbol{k}} \times \boldsymbol{u}_i = -\nabla p_i, \tag{2.1}$$

$$h_{it} + \nabla \cdot (h_i \boldsymbol{u}_i) = 0, \tag{2.2}$$

where the subscript $i = 1$ (2) denotes the upper (lower) layer, $\boldsymbol{u} = (u, v)$ is the horizontal velocity vector, f is the Coriolis parameter, ∇ is the horizontal differential operator and $\hat{\boldsymbol{k}}$ is the vertical unit vector. The layer's reduced pressure (p_i, the pressure

divided by density) and depth (h_i) are related by the hydrostatic equation:

$$g'\nabla h_1 = -g'\nabla h_2 = \nabla(p_1 - p_2), \tag{2.3}$$

where $g' \equiv g(\rho_2 - \rho_1)/\rho_1$ is the reduced gravity. PV is conserved in each layer,

$$(\partial_t + \boldsymbol{u}_i \cdot \nabla)\, q_i = 0, \quad q_i \equiv \frac{f + \hat{\boldsymbol{k}} \cdot \nabla \times \boldsymbol{u}_i}{h_i}. \tag{2.4}$$

The flow whose linear-stability characteristic we investigate is trapped at the interface between two semi-infinite regions of constant PV, $q_{1j} \equiv f/H_{1j}$, where j denotes the side of this PV front (1 being south, $y < 0$), and H_{1j} the fluid depth at $y \to \mp\infty$ (figure 1). Requiring that the flow be x-independent, continuous both in layer depth and velocity, steady, geostrophic, $u_2 = 0$, the upper-layer depth is

$$h_1 = \begin{cases} H_{11}\left[\left(\left(H_{12}/H_{11}\right)^{1/2} - 1\right)\exp(y/R_{d,1}) + 1\right] & \text{for } y < 0 \\ H_{12}\left[\left(\left(H_{11}/H_{12}\right)^{1/2} - 1\right)\exp(-y/R_{d,2}) + 1\right] & \text{for } y > 0, \end{cases} \tag{2.5}$$

and the geostrophic jet velocity is

$$u_1 = -\frac{g'}{f}\frac{\mathrm{d}h_1}{\mathrm{d}y} = U_0 \begin{cases} \exp(y/R_{d,1}) & \text{for } y < 0 \\ \exp(-y/R_{d,2}) & \text{for } y > 0 \end{cases} \tag{2.6}$$

where

$$U_0 = \left(g'H_{11}\right)^{1/2} - \left(g'H_{12}\right)^{1/2} \text{ and } R_{d,j} \equiv (g'H_{1j})^{1/2}/f, \tag{2.7}$$

are the jet maximum speed and the (different) deformation radii on each side of the front.

We non-dimensionalize the governing equations similar to Williams (1991), by transforming

$$t \to \frac{tR_d}{U_0},\ (x,y) \to (x,y)R_d,\ (u,v) \to (u,v)U_0,\ h_i \to h_i\bar{H}, \text{and } \psi_i \to p_i(g'\bar{H})^{1/2}U_0, \tag{2.8}$$

where

$$\bar{H} \equiv (H_{11} + H_{12})/2,\ R_d \equiv \left(g'\bar{H}\right)^{1/2}/f, \tag{2.9}$$

and $\bar{H}$ is the y-averaged upper-layer depth and R_d the radius of deformation based on $\bar{H}$. The non-dimensional Rossby number, $\epsilon \equiv |U_0|/fR_d$, is a measure of the strength and asymmetry of the flow.

It is convenient to define the following non-dimensional variables:

$$Q_j \equiv \frac{\bar{H}}{H_{1j}},\ \epsilon\eta_j \equiv h_1 - Q_j^{-1} \tag{2.10}$$

so that the hydrostatic relation becomes

$$\nabla(\psi_1 - \psi_2) = \nabla\eta. \tag{2.11}$$

Q_j and η_j are the scaled constant PV and interface displacement on either side of the front and ψ_i is the scaled reduced pressure in each layer.

The resulting non-dimensional governing equations ((2.1)–(2.2)) are

$$\epsilon\,(\partial_t + \boldsymbol{u}_i \cdot \nabla)\,\boldsymbol{u}_i + \hat{\boldsymbol{k}} \times \boldsymbol{u}_i = -\nabla\psi_i, \tag{2.12}$$

$$\epsilon\left(\eta_{j,t} + \nabla \cdot (\eta_j \boldsymbol{u}_1)\right) + Q_j^{-1}\nabla \cdot \boldsymbol{u}_1 = 0, \tag{2.13}$$

$$\epsilon\left(\eta_{j,t} + \nabla\cdot(\eta_j \boldsymbol{u}_2)\right) - (r - Q_j^{-1})\nabla\cdot\boldsymbol{u}_2 = 0, \tag{2.14}$$

and the non-dimensional PV is given by

$$q_1 = \frac{1 + \epsilon\nabla\times\boldsymbol{u}_1}{Q_j^{-1} + \epsilon\eta_j}, \quad q_2 = \frac{1 + \epsilon\nabla\times\boldsymbol{u}_2}{r - Q_j^{-1} - \epsilon\eta_j}, \tag{2.15}$$

where $r \equiv H_T/\bar{H}$, the ratio of the total fluid depth to the mean upper-layer depth. Thus, the two parameters describing the flow are ϵ and r.

The non-dimensional mean-flow variables, denoted by an overbar, are calculated from (2.5)–(2.6),

$$\bar{u}_1 = -\bar{\psi}_{1y} = \exp(-\alpha_j|y|), \ \bar{\psi}_1 = \operatorname{sign}(y)\left[\frac{1}{\alpha_j}\left(\exp(-\alpha_j|y|) - 1\right)\right], \tag{2.16}$$

$$\bar{\eta}_j = \operatorname{sign}(y)\frac{\exp(-\alpha_j|y|)}{\alpha_j}, \ \bar{v}_1 = 0, \ \bar{v}_2 = \bar{u}_2 = \bar{\psi}_2 = 0,$$

where $\alpha_j = R_d/R_{d,j} = Q_j^{1/2}$ so that $\sqrt{2} \geqslant 1/\alpha_j \geqslant 0$. The non-dimensional layer depths are given by

$$\bar{h}_1 = \frac{1}{Q_j} + \epsilon\bar{\eta}_j \text{ and } \bar{h}_2 = r - \bar{h}_1. \tag{2.17}$$

From the definitions of ϵ and Q_j, Williams (1991) derived

$$\epsilon = 1/\alpha_1 - 1/\alpha_2, \quad (1/\alpha_1)^2 + (1/\alpha_2)^2 = 2. \tag{2.18}$$

Without loss of generality we choose the north side ($y > 0$) to be shallower, $H_{11} > H_{12}$ (or $\alpha_2 > \alpha_1$).

Up to this point no assumption has been made about the magnitude of ϵ, which, over the whole range of possible upper-layer PV distributions, varies from zero to $\sqrt{2}$. Special cases of the PV-front model presented here were considered in the past: when $\epsilon = \sqrt{2}$, $H_{12} = 0$, so that $h_1 = 0$ for $y > 0$ in (2.5) is the outcropping (or density) front studied by KPS. The QG limit is $\epsilon = 0$. The above model in the limit $r \to \infty$ ($1\frac{1}{2}$-layer) was studied for $\epsilon = \sqrt{2}$ by Paldor (1983), for variable ϵ by Williams (1991) and for $\epsilon = 0$ by Pratt & Stern (1986).

In the limit $\epsilon \to 0$, the potential vorticity can be expanded to the first order in ϵ,

$$q_1 = 1 + \epsilon(\nabla^2\psi_1 - (\psi_1 - \psi_2)), \quad (r-1)q_2 = 1 + \epsilon\left(\nabla^2\psi_2 + \frac{(\psi_1 - \psi_2)}{(r-1)}\right) \tag{2.19}$$

satisfying

$$\left(\partial_t + \boldsymbol{u}_{i,g}\cdot\nabla\right) q_i = 0 \tag{2.20}$$

with the geostrophic advective flow

$$\hat{\boldsymbol{k}}\times\boldsymbol{u}_{i,g} = -\nabla\psi_i, \tag{2.21}$$

which is the QG approximation (Pedlosky 1987). In this approximation the non-dimensional mean flow is given by (2.16)–(2.17) with $\alpha_1 = \alpha_2 = 1$. We note that when $\epsilon = 0$ there is no flow, since then the dimensional $h_1 = H_{12} = H_{22}$ is a constant. In the QG approximation, by setting the value of the PV to be different on each side of the front, the jet speed is

$$U_0 = \left(\frac{g'f}{q_{11}}\right)^{1/2} - \left(\frac{g'f}{q_{12}}\right)^{1/2} = \epsilon(g'\bar{H})^{1/2}. \tag{2.22}$$

Thus we can approximate the shallow-water PV front in the QG approximation by the choice of U_0. The approximation, of course, worsens with the increase in size of ϵ.

2.1. *Linearized perturbation equation of a PV front*

In order to assess the linear stability of this flow we superimpose an infinitesimal, normal-mode, perturbation on the mean flow so that u_i, v_i and ψ_i all have the form $\theta = \mathrm{Re}\left(\bar{\theta}(y) + \theta(y)\exp(\mathrm{i}k(x - ct))\right)$, i.e. the sum of an x-averaged mean flow (given in (2.16)–(2.17)) and a wave-like infinitesimal perturbation. Since we are considering an f-plane shallow-water model, the conditions for the hydrostatic balance to be applicable are that $\epsilon H^2/L^2 \ll 1$, which for the $O(1)$ Rossby number model considered here, implies that our model is valid so long as $k < R_d/\bar{H}$ (or in dimensional form $k < 1/\bar{H}$).

Linearizing the momentum and PV equations in the upper layer about the mean flow results in the following system:

$$\epsilon(\bar{u}_1 - c)u_1 + (\epsilon\bar{u}_{1y} - 1)\hat{v}_1 = -\psi_1, \tag{2.23}$$

$$-k^2\epsilon(\bar{u}_1 - c)\hat{v}_1 + u_1 = -\psi_{1y}, \tag{2.24}$$

and

$$k^2\hat{v}_1 + u_{1y} = Q_j(\psi_2 - \psi_1), \tag{2.25}$$

where $\hat{v}_1 \equiv v_1/\mathrm{i}k$. In the lower layer, where there is no mean flow, substituting the linearized momentum equations into the linearized mass conservation equation gives

$$\left(\bar{h}_2\psi_{2y}\right)_y + \left(\epsilon^2k^2c^2 - 1 - k^2\bar{h}_2 + \frac{\bar{u}_1}{c}\right)\psi_2 = (\epsilon^2k^2c^2 - 1)\psi_1. \tag{2.26}$$

We thus have a fourth-order system of ordinary differential equations with four unknowns and an eigenvalue, c. The solution we are seeking is required to vanish away from the front ($y \to \pm\infty$, thus we are restricting ourselves to solutions with finite energy per unit length of front). At the front ($y = 0$) the matching conditions differ between the cases $\epsilon < \sqrt{2}$ and $\epsilon = \sqrt{2}$, due to the vanishing of the upper layer in the latter case. For the non-outcropping PV front ($\epsilon < \sqrt{2}$) the boundary conditions are that all the perturbation amplitudes, except u_1, are continuous at $y = 0$. For the outcropping front ($\epsilon = \sqrt{2}$), the upper-layer boundary is at $y = 0$ and the boundary condition there was derived by KPS based on the regularity of (2.23) at $y = 0$, so that

$$\epsilon(\bar{u}_1 - c)u_1 + \psi_1 = 0. \tag{2.27}$$

Since in this case, the lower-layer solution for ψ_2 at $y > 0$ is a decaying exponential (by (2.26)), continuity of ψ_2 at $y = 0$ implies

$$\psi_{2y} + k\psi_2 = 0. \tag{2.28}$$

Thus, the boundary conditions, as well as the mean flow, pass continuously from the non-outcropping to the outcropping front, and we can therefore expect the instability properties to also be continuous. The method of solution we employed to solve (2.23)–(2.26) with the above boundary conditions is presented in Appendix A.

Because we are considering only trapped modes, the boundary conditions eliminate solutions representing free waves that are finite when $y \to \pm\infty$. Such gravity waves are free when their Doppler-shifted frequency ($\omega_0 = k(c - \bar{u})$) exceeds the effective Coriolis frequency, $f_{eff} = f + \hat{\boldsymbol{k}} \cdot \nabla \times \boldsymbol{u}/2$ and are trapped (have a complex

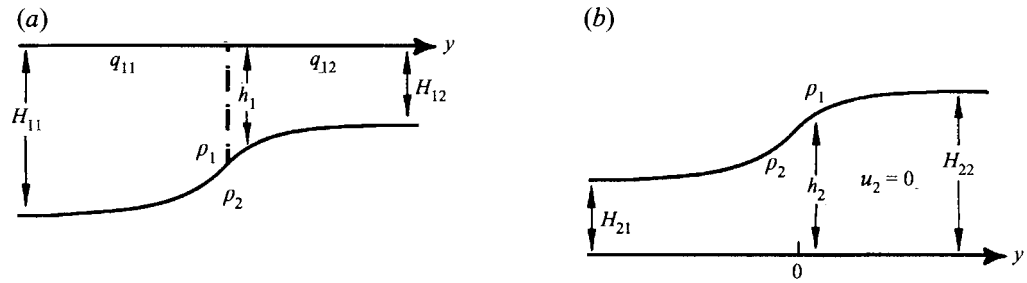

FIGURE 2. (*a*) The upper- and (*b*) lower-$1\frac{1}{2}$-layer models that are used to interpret the instabilities present in the 2-layer model of figure 1. The jet structure of the upper-layer model is identical to that of the 2-layer model. Both $1\frac{1}{2}$-layer models are stable to normal-mode perturbation, while the 2-layer model is unstable.

meridional wavenumber) where $\omega_0 < f_{eff}$. For trapped gravity waves that have a non-zero amplitude within the jet (where $\omega_0 > f_{eff}$) but decay outside the jet (where $\omega_0 < f_{eff} = f$), the local mean-flow vorticity $\zeta = \hat{\boldsymbol{k}} \cdot \nabla \times \bar{\boldsymbol{u}}_1$ (i.e. $\zeta = -\bar{u}_{1y}$ in our case) has to be negative. This occurs for all values of ϵ on the south side of the PV front ($y < 0$). However, on the north side of the PV front the gravity waves are always free, except for the outcropping front ($\epsilon = \sqrt{2}$), where these waves do not exist for $y > 0$. Thus trapped gravity waves can only be found for the outcropping front configuration. Trapped vortical waves, on the other hand, can be present in both layers and for all ϵ, as is shown in the next section.

3. Some relevant results from the $1\frac{1}{2}$-layer models

In order to interpret the instabilities of the 2-layer model, the wave–wave resonance that gives rise to the instabilities has to be elucidated (Hayashi & Young 1987; Sakai 1988). We follow Sakai (1988) and decompose the 2-layer model into two $1\frac{1}{2}$-layer models; one with an infinite bottom layer and the other with an infinite upper layer (figure 2). The lower-layer models are stable by Ripa's (1983) stability criteria for all ϵ. The upper-layer models are stable for all ϵ except when $\sqrt{2} > \epsilon^2 > 0.4$, where an instability arises from a resonant interaction of a gravity wave, that is free on the north side of the front, and a trapped vortical wave (Ford 1993). Our boundary conditions preclude such instabilities and the modes observed in the upper-layer models are stable for all ϵ. The modes found in these models are expected to be similar, but not identical, to those of the 2-layer modes given that they represent the limit of the latter when a layer becomes infinite. An instability in the 2-layer model is expected when waves of the upper- and lower-layer models have a similar frequency, $\omega = kc$.

3.1. *Upper-layer modes*

The upper-layer model consists of (2.23)–(2.25) with $\psi_2 = 0$ (figure 2*a*). The mean flow is identical to that of the 2-layer model (2.6). The modes and their dispersion relation (figure 3, bold lines) were studied previously for all ϵ: Pratt & Stern (1986) studied the QG case ($\epsilon = 0$), Williams (1991) studied it for $0 < \epsilon < \sqrt{2}$ and Paldor (1983) for the outcropping front ($\epsilon = \sqrt{2}$). The eigenmodes associated with the different cases are depicted in figure 4(*a–d*). In particular the QG dispersion relation and eigenmode can be derived analytically ($\epsilon = 0$ line in figures 3*d* and 4*a*),

$$\omega = k\left(1 - (k^2 + 1)^{-1/2}\right), \quad \psi_1 = A\mathrm{e}^{-\beta|y|} \tag{3.1}$$

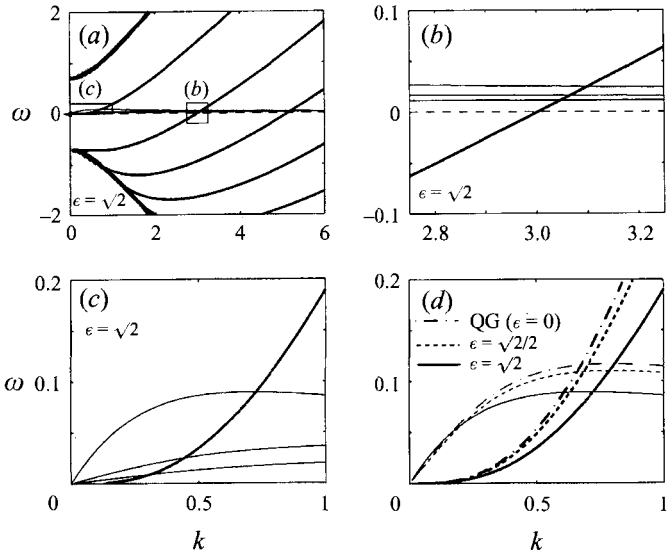

FIGURE 3. The dispersion relation (DR) of the upper- and lower-1½-layer trapped modes. Bold lines are the DR of upper-layer modes, thin lines represent DR of lower-layer modes and the dashed line in (*a*, *b*) is zero. (*a*) The outcropping front case of which (*b*) is a magnification of the short-wave region and (*c*) is a magnification of the long-wave one. Only the three gravest (in meridional structure) lower-layer modes are shown. Where the DR of lower- and upper-layer modes approach each other an instability is expected. The heavy lines denote the boundaries beyond which free waves are found (Paldor 1983). (*d*) The DR of the upper-layer modes and the gravest lower-layer mode for three values of ϵ. Notice the similarity between the DR of the QG and the outcropping front.

where $\beta \equiv (k^2+1)^{1/2}$ and A is the (arbitrary) infinitesimal amplitude of the perturbation.

Sakai (1988) suggested the use of the pseudo-momentum to differentiate between gravity and Rossby waves in a baroclinic shear flow. We show in Appendix B that for the upper-layer model, Sakai's conjecture fails and we therefore use the continuity in structure of the eigenmodes and dispersion relation (DR) of the modes as ϵ changes to differentiate between the vortical and gravity waves; in the QG limit only vortical waves are present. Thus we physically interpret the modes found by Paldor (1983) ($\epsilon = \sqrt{2}$) as follows: the gravest mode is a vortical wave, since we can trace this mode from $\epsilon = 0$ (QG) to $\epsilon = \sqrt{2}$ in both DR and structure (figures 3*d* and 4*a–c*). The other modes found for $\epsilon = \sqrt{2}$ are trapped gravity waves that, as argued in § 2, are unique to the outcropping fronts. The DR of the gravity waves emanates from the free-wave DR, $\omega = -(1+k^2)^{1/2}$ (heavy line in figure 3*a*), and the eigenfunctions differ from those of the vortical waves, for example, in that the number of points where the eigenfunction vanishes increases with mode number (figure 4*c–d*; Paldor 1983).

As ϵ is changed from zero the vortical mode loses the north–south symmetry it had in the QG model until its northern side disappears as the interface intersects (figure 4*a–c*). The DR curves of the vortical modes for different values of ϵ all emanate from the origin, $k = 0$, they then spread apart from each other as k increases (figure 3*d*), but they have the same limit as $k \to \infty$ (not shown here, Williams 1991). For all $\epsilon < \sqrt{2}$ the PV gradient supporting the vortical modes is concentrated at $y = 0$, $q_{1y} = \delta(y)(q_{12} - q_{11})$. Notice, however, that when $\epsilon = \sqrt{2}$ (outcropping front)

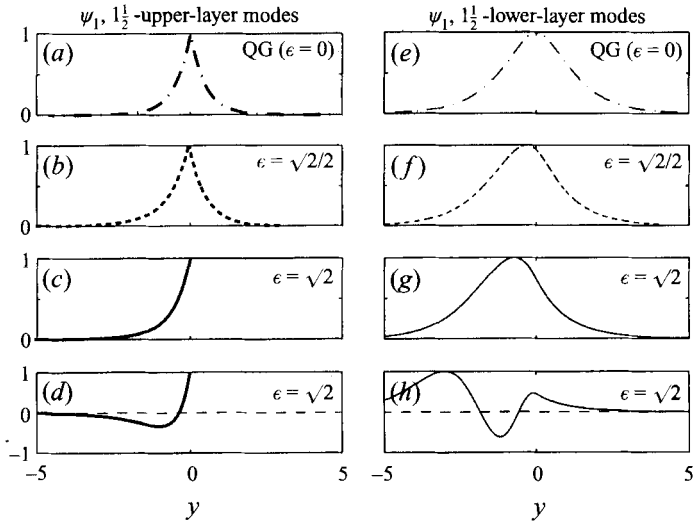

FIGURE 4. The eigenmode structure corresponding to different dispersion curves of figure 3 (same line pattern), for $k = 1$ and $r = 4$. (*a–c*) Upper-layer vortical modes with different values of ϵ. (*d*) The first gravity mode of the outcropping front. (*e–g*) The first lower-layer model vortical modes with different values of ϵ. (*h*) The third lower-layer vortical mode of the outcropping front. The amplitudes are normalized with each modes maximum amplitude.

the vortical mode exists even though the PV gradient in the upper layer apparently vanishes. Using the fact that the results are continuous as function of ϵ we interpret the layer intersection point at $y = 0$, when $\epsilon = \sqrt{2}$, as a PV discontinuity from the finite upper-layer PV for $y < 0$ to an infinitely thin layer with an infinite PV at $y > 0$. This provides the gradient necessary for the existence of a vortical wave. This interpretation of the PV front is similar to that which is used for continuously stratified QG models (Bretherton 1966*a*).

3.2. *Lower-layer modes*

The lower-layer model consists of (2.26) with $\psi_1 = 0$ (figure 2*b*). We choose $r = 4$, so as to be consistent with the 2-layer profiles analysed in the next section. The only modes present are vortical modes owing to the variation in layer depth, with no mean flow; they are trapped in the area where the layer depth varies and are similar to topographic Rossby waves. Unlike the upper-layer model, more than one vortical mode exists in the lower layer.

The DR (figure 3*d*) and eigenmode structure (figure 4*e–g*) vary continuously as a function of ϵ for a single mode. The phase speed (not shown) of different modes differs mostly at low wave numbers, while at large wave numbers the phase speed of all the modes asymptotes to zero. The structure of the different modes as a function of ϵ involves a shift in the maximum amplitude to the south side and a loss of the symmetry found in QG (figure 4*e–g*). For a given ϵ the modes vary in the number of times their amplitude is zero, having more such points as the frequency decreases (figure 4*g*, *h*).

As with the upper model, the QG solution can be obtained analytically; the governing equation ((2.26) with $\psi_1 = 0$ and $\epsilon = 0$) is

$$(\bar{h}_2\psi_{2y})_y + \left(-1 - k^2\bar{h}_2 + \frac{e^{-|y|}}{c}\right)\psi_2 = 0, \tag{3.2}$$

with $\bar{h}_2 = r - 1$. Changing the independent variables in each half-plane to $z \equiv e^{-|y|}$ in (3.2) gives

$$z^2\psi_{2zz} + z\psi_{2z} + \left(\frac{z}{(r-1)c} - k^2 - \frac{1}{r-1}\right)\psi_2 = 0, \tag{3.3}$$

whose solution is (Kamke 1951)

$$\psi_2 = AJ_\nu\left(2\left(\frac{z}{(r-1)c}\right)^{1/2}\right); \quad \nu = 2\left(k^2 + \frac{1}{r-1}\right)^{1/2}, \tag{3.4}$$

where A is the arbitrary infinitesimal amplitude of the perturbation and J_ν the Bessel function of the first kind of order ν. Requiring that ψ_2 be continuous at the front ($y = 0$; $z = 1$) and using the symmetry of ψ_2 at the origin, we find c as the root of the transcendental equation

$$\nu J_\nu(a) - aJ_{\nu+1}(a) = 0; \quad a \equiv 2(c(r-1))^{-1/2}. \tag{3.5}$$

We notice first that the dynamics of the vortical wave, as that of the mean flow, changes continuously from $\epsilon = 0$ to, and including, $\epsilon = \sqrt{2}$. This will also be the case when a second active layer is introduced, permitting us to identify QG dynamics, and to extrapolate the insight derived from stability theorems derived in the QG model to the outcropping shallow-water model.

Given a wavenumber, we can now predict the type of baroclinic instability likely to occur in the two-layer model of figure 1; at the long-wave end, the vortical waves of the upper- and lower-layer models have similar frequencies (figure 3*d*) and we can therefore expect a QG baroclinic instability for all ϵ. At higher wavenumber, when the frequency of the upper-layer gravity modes crosses zero and becomes positive, a resonant interaction with lower-layer vortical modes becomes possible. This short-wave interaction can occur only for the outcropping front and is ageostrophic, and thus is not present in the QG system.

We observe that more than one lower-layer vortical mode has the potential to resonate with the upper-layer modes. Sakai (1988) found that the modes most likely to interact are the ones having similar spatial structure. We thus expect the gravest lower-layer vortical mode to resonate with the upper-layer vortical mode (compare figures 4*a–c* and 4*e–g*). In the case of the outcropping front the upper-layer gravity mode has a structure different from the lower-layer vortical modes (figures 4*d* and 4*g*, *h*) suggesting that it may be able to interact with more than a single mode. The next section confirms these predictions.

4. Instability of the 2-layer model

The growth-rate curves of the instabilities present in the 2-layer model (figure 5) confirm the predictions of the previous section. A long-wave instability exists for all ϵ, and changes continuously as a function of ϵ while short-wave instabilities can be found in the intersecting front case only.

4.1. *Long-wave quasi-geostrophic instability*

The long-wave instability is found for all ϵ and is therefore a QG instability, that is an interaction of two vortical modes; in our model, the upper-layer vortical mode resonates with a lower-layer one. The structure of the unstable modes (figure 6) changes continuously with ϵ and closely resembles the stable $1\frac{1}{2}$-layer modes (figure 4).

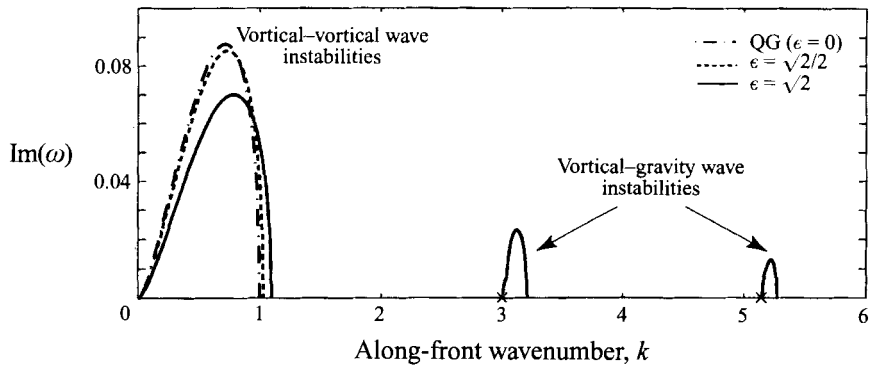

FIGURE 5. Growth rates of the instabilities present in the 2-layer model, $r = 4$. For all values of ϵ, the model exhibits the long-wave (QG) baroclinic instability. In addition, an ageostrophic vortical–gravity wave instability exists for the outcropping front. $\times$ denotes the locations where the frequency of the upper-layer gravity-wave modes becomes positive and can thus resonate with the lower-layer vortical modes. The growth rate is non-dimensionalized with $U_0/R_d = \epsilon/f, k$ with k_d.

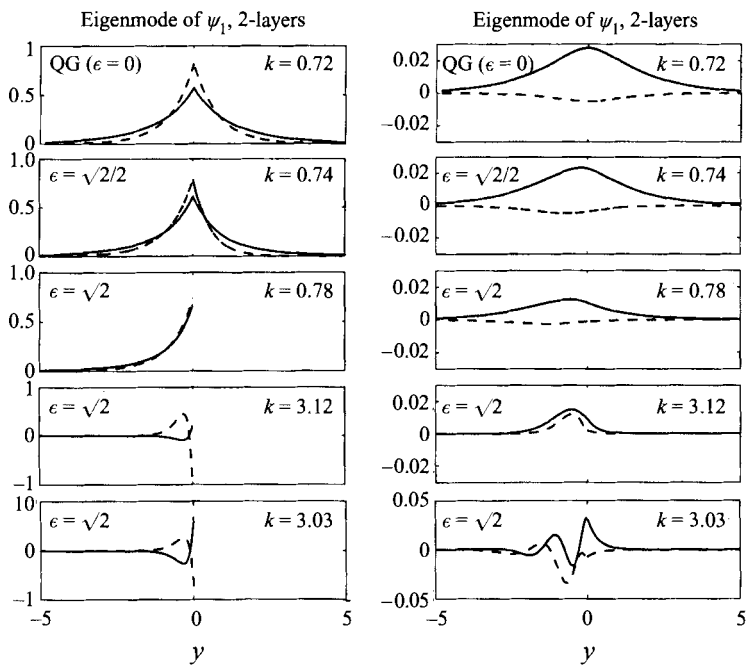

FIGURE 6. Structure of the eigenmodes of the 2-layer instabilities corresponding to the most unstable wave of figure 5. Solid and broken lines denote the real and imaginary parts respectively. The amplitudes of the eigenmodes are different for each case but the ratio of ψ_1 to ψ_2 is preserved. Notice the similarities with the $1\frac{1}{2}$-layer eigenmodes (figure 4).

We observe that in all the cases only the gravest lower-layer vortical mode resonates, which can be explained by the similarity of its structure with that of the upper-layer mode (figures 4*c* and 4*g*). Also, the ratio of depth-weighted pressures, $\psi_1/((r-1)\psi_2)$, is $O(1)$, signifying that the perturbation energy is of the same order of magnitude in both layers.

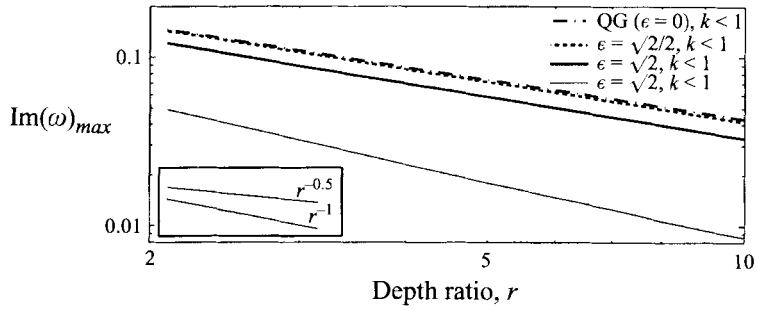

FIGURE 7. Logarithmic plot of the unstable modes maximum growth rate as a function of $r = H_T/\bar{H}$. The top three curves are the maximum growth rates for the long-wave instability and the lower curve is for the short-wave instability.

The change in the maximum growth rate as a function of the depth ratio, r, is similar for all ϵ (figure 7), with a decay rate varying from $r^{-0.78}$ for QG to $r^{-0.83}$ for $\epsilon = \sqrt{2}$.

4.2. *The $k \to 0$ limit*

In the limit $k \to 0$, the dimensional growth-rate of a baroclinic instability for any two-layer, shallow-water model with a jet of finite horizontal extent confined in the upper layer is (G. R. Flierl, personal communication, see also KPS)

$$\mathrm{Im}(\omega) = \frac{k}{2r}\left(\int_{-\infty}^{\infty} \bar{h}_1 \bar{u}_1^2 \mathrm{d}y\right)^{1/2}. \tag{4.1}$$

This is in good agreement with the growth rates displayed in figure 5 for all ϵ.

Also, in this limit, the energetics of the instability can be found analytically using an expansion in the wavenumber k. The energy transfer equation has been considered in detail in KPS, and except for minor details is identical to the one in our study. Their equation (4.33) becomes using our scaling

$$\frac{\mathrm{d}}{\mathrm{d}t}\int_{-\infty}^{\infty} \mathscr{E}\mathrm{d}y = \frac{\mathrm{Im}(\omega)}{2}\left\{\int_{-\infty}^{\infty} \bar{h}_1 \bar{u}_{1y}^2 \mathrm{d}y + \int_{-\infty}^{\infty} \bar{u}_1^2 \mathrm{d}y\right\} + O(k^2) \tag{4.2}$$

where $\mathscr{E}$ is the non-dimensional perturbation energy

$$\mathscr{E} = \tfrac{1}{2}\langle \bar{h}_1 (u_1^2 + v_1^2) + \bar{h}_2 (u_2^2 + v_2^2) + (\psi_1 - \psi_2)^2 + 2\bar{u}_1 u_1 (\psi_1 - \psi_2)\rangle, \tag{4.3}$$

and angle brackets denoting an average over an along-front wavelength. The last term of (4.3), a term that can potentially be negative (Ripa 1983; Hayashi & Young 1987), is, to first order in k, identically zero when integrated over the whole domain. The two terms on the right-hand side of (4.2) are the barotropic and baroclinic energy conversion terms respectively (KPS). An interesting result is that these terms are of equal magnitude for all ϵ, although the instability we observe requires the presence of a second active layer (i.e. is baroclinic). It suggests that the energetics of the instability alone cannot be used to differentiate between barotropic and baroclinic instabilities.

4.3. *Short-wave ageostrophic instability*

Short-wave instabilities exist only for the intersecting front ($\epsilon = \sqrt{2}$). We analyse only the longest ones since the others are similar in properties and the application of the shallow-water approximation is not strictly valid when $k \sim R_d/\bar{H}$.

The instabilities are surface trapped, with $\psi_1/((r-1)\psi_2)$ of $O(0.01)$ (figure 6). The growth rate is smaller than the long-wave instability by about 60%. The unstable eigenmodes are reminiscent of the upper-$1\frac{1}{2}$-layer gravity mode and lower-$1\frac{1}{2}$-layer vortical mode of figures 4(*c*, *d*) and 4(*g*, *h*). The instability occurs very close to the wavenumber (k) where the frequency of the $1\frac{1}{2}$-layer gravity modes becomes positive (denoted by $\times$ in figure 5 where only the first two are shown), making it possible for an upper-layer gravity mode to resonate with a lower-layer vortical mode. The resonance is not isolated to the gravest lower-layer mode: the side lobes in the growth-rate curves (figure 5) are due to resonant interaction with other lower-layer vortical modes. As seen in figure 6, two different lower-layer vortical modes interact with the upper-layer gravity mode for $k = 3.03$ and $k = 3.12$, both of which are part of the first short-wave instability curve (e.g. the slight 'knee' in the DR near $k = 3$ in figure 5). We conclude that the short-wave instabilities are ageostrophic, resulting from a resonance between gravity and vortical modes.

We have shown that an extension of the QG instability exists at the intersecting front. A necessary condition for the existence of a baroclinic instability in the QG model (the Charney–Stern theorem) is that the PV gradient reverses between the upper and lower layers. In our case for all $\epsilon < \sqrt{2}$,

$$q_{1y} = \delta(y)(q_{12} - q_{11}) > 0, \tag{4.4}$$

while in the lower layer,

$$q_{2y} = \frac{-f\bar{h}_{1y}}{\bar{h}_1^2} < 0. \tag{4.5}$$

The case $\epsilon = \sqrt{2}$ is subtle. The mean flow, apparently, does not satisfy the condition for instability, as the upper layer is of constant PV (q_{11}). This has led numerous previous authors (e.g. KPS; Sakai 1988; Barth 1989) to interpret the long-wave instability of the intersecting front as ageostrophic, i.e. requiring dynamics not present in QG. However, in our model, since the intersecting front is found by taking the regular limit $H_{12} \to 0$, the upper-layer PV jump becomes infinite, still satisfying the reversal, and thus confirming the QG nature of the instability. The situation is similar to the continuously stratified Eady model, where the PV gradient occurs on the top and bottom boundaries (Bretherton 1966*a*). The upper-layer jump in PV in the intersecting front case provides the gradient which supports the vortical wave in the upper layer (§3.1). The potential of interpreting shallow water instabilities from insight derived in the QG framework is not limited to baroclinic instability, as we show in the next section.

5. Application to a barotropic shear flow

In the previous sections we have demonstrated that the Charney–Stern theorem, namely that the reversal of vertical PV gradient is a necessary condition for instability, is useful in predicting the instability of an intersecting shallow-water front, where the upper-layer PV gradient is isolated at the intersection point. Similarly, we can expect in barotropic flows, such as that investigated by Griffiths *et al.* (1982, hereafter GKS, see figure 8*a*), that the Rayleigh–Kuo theorem, namely that the horizontal PV gradient must reverse for instability to occur, will be satisfied by the flow when the intersection points are taken into account. The instability is also quasi-geostrophic in nature, in contrast to previous interpretations (e.g. Killworth 1983; GKS).

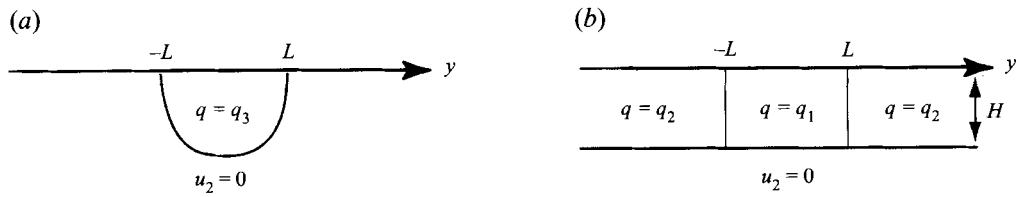

FIGURE 8. (*a*) The shallow-water model studied by Griffiths *et al.* (1982) and (*b*) its QG analogue. The QG solution has similar growth rates and structure to that of GKS's model when the PV jump across the front is such that the maximum current velocity (U_0), length ($R_d = (g'H)^{1/2}/f$) and depth (H) scales are the same.

In GKS, a long-wave instability is observed in a $1\frac{1}{2}$-layer shallow-water model of a double front (intersecting in two places) with constant PV. We develop a simple QG analogue to the shallow-water model of GKS (figure 8*b*) which we solve analytically (following Nakamura 1993). The upper layer is divided into three regions of constant PV with the outer two having the same PV in order to preserve the symmetry found in GKS. Assuming geostrophy, the dimensional mean flow is

$$u_1 = U_0 \begin{cases} -\exp((y+L)/R_d) & \text{for } y < -L \\ \dfrac{\sinh(y/R_d)}{\sinh(L/R_d)} & \text{for } -L < y < L \\ \exp(-(y-L)/R_d) & \text{for } L < y \end{cases} \tag{5.1}$$

where

$$U_0 = \tfrac{1}{2} H R_d (q_1 - q_2)\left(1 - \exp(-2L/R_d)\right) \text{ and } R_d \equiv (g'H)^{1/2}/f,$$

are the maximum speed of the flow and the radius of deformation. The potential vorticity gradient,

$$q_y = \begin{cases} \delta(y)(q_1 - q_2) & \text{for } y = -L \\ -\delta(y)(q_1 - q_2) & \text{for } y = L, \end{cases} \tag{5.2}$$

satisfies the necessary condition for normal-mode instability. Solving for a normal-mode perturbation, $\psi = \Psi(y) + \mathrm{Re}[\psi(y)\exp(ik(x-ct)]$, the perturbation-PV conservation equation is

$$\frac{\mathrm{d}^2\psi}{\mathrm{d}y^2} - \mu^2\psi = 0; \quad \mu \equiv (k^2 + R_d^{-2})^{1/2} \tag{5.3}$$

whose solutions are exponentials with an e-folding length μ^{-1}. The matching conditions at the PV fronts require continuity in the along-front velocity (geostrophic and ageostrophic), implying that both ψ and

$$(u_1 - c)\frac{\mathrm{d}\psi}{\mathrm{d}y} + \left(f + \frac{\mathrm{d}u_1}{\mathrm{d}y}\right)\psi$$

are continuous across the fronts (Nakamura 1993). The problem is reduced to solving a quadratic equation for c.

The growth rate, its dependence on the current width, L (figure 9), and the structure and symmetries of the eigenmodes (not shown) are all similar to those found by GKS for the case of a constant-PV front (compare figure 9 here with their figures 5 and 6). We thus conclude that the instability studied by GKS is a shallow-water extension of the QG instability arising from a resonant interaction of two vortical modes. We emphasize that in order for the QG model to approximate well the shallow-water

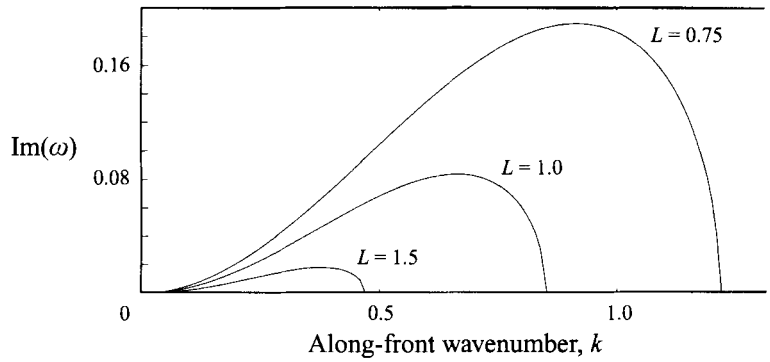

FIGURE 9. The growth rate of the long-wave instability as a function of the wavenumber k for currents with three different widths (L). The growth rate is non-dimensionalized with U_0/R_d, k and L with R_d.

results, the depth, length and velocity scales should be matched, not the actual PV distribution, which is different in the two models.

The short-wave ageostrophic instabilities of the GKS profile were studied by Hayashi & Young (1987) for the case of zero PV. They found instabilities due to resonance between the QG modes and ageostrophic gravity waves (their figure 2). Their growth-rate curves for the barotropic instabilities are strikingly similar to the baroclinic growth-rate curves of figure 5 here; besides the long-wave instability curve, they find several short-wave instabilities whose growth rates decrease with k.

Killworth (1983) found a long-wave instability in a $1\frac{1}{2}$-layer shallow-water model of an intersecting front, when the PV gradient on the south side of the front was negative (i.e. figure 2*a* with $H_{12} = 0$ and $\partial q_{11}/\partial y < 0$). Interpretation of the intersecting point as a δ-function in PV gradient supplies the reversal of PV needed to satisfy the Rayleigh–Kuo theorem, again making it possible to interpret this instability in the context of the QG dynamics, in contrast to Killworth's interpretation.

6. Discussion and conclusions

We have found, in both baroclinic and barotropic shear flows, that long-wave instabilities, previously believed to involve dynamics not present in QG flows, are in effect extensions of QG instabilities. The key point, long realized in continuously stratified QG flows, is the connection between density and PV fronts. This connection extends the physical insight of the stability of shear flows from QG to shallow water.

Observation of Gulf-Stream meanders (Watts & Johns 1982; Tracey & Watts 1986) and of coastal upwelling regions (e.g. Barth 1994 and references therein) have found both long- and short-wave instabilities. Also, while the long-wave instabilities are observed to extend throughout the fluid, the short-wave instabilities are surface trapped (Barth 1994). Both aspects are captured by the simple intersecting model of KPS whose analysis we have extended here. The growth rate of the long-wave instabilities is of similar magnitude to those observed (for a detailed comparison with instabilities of the Gulf Stream see KPS). However, in contrast to our findings, in a continuously stratified horizontally bounded model, Barth (1994) finds that the short-wave instability grows faster than the long-wave one while Paldor & Ghil (1991) obtained the same result for a two-layer shallow-water model of a coastal front.

Two-dimensional continuously stratified primitive equation models (Stone 1970; Nakamura 1988) have been found to support both a long-wave QG instability and a short-wave surface-trapped vortical–gravity wave interaction instability that are connected to the presence of critical levels, where the governing equations encounter singularities. As was pointed out by Bretherton (1966*b*), critical levels are not present in layer models, but the similarities between the instabilities found here and those found in the continuously stratified fluid suggests that the physics underlying the instabilities are the same.

Sakai (1988) predicted the existence of vortical–gravity wave interaction in the KPS profile found here, but mistook the nature of the instability found in KPS. His conjecture that the instabilities can be identified using momentum analysis is limited to cases where the QG and shallow-water mean profiles are identical in their PV distribution.

Our results suggest that the quasi-geostrophic approximation may be more applicable to frontal problems than previously thought. For example, studies of the Gulf Stream using contour dynamics (Pratt & Stern 1986; Meacham 1991) where the fluid is divided into regions of constant PV, may be more realistic than previously realized. This is encouraging because of the relative simplicity of QG theory. When QG theory is used, the PV distribution should be such that the length, height, and velocity scales match those of the flow of interest; the actual values of the PV may be different.

On the other hand, we expect that for unstable fronts, the nonlinear evolution will differ between the QG and shallow-water approximation. For example, differences are to be expected in the evolution of mesoscale eddies. While the QG approximation does not discriminate between cyclones and anti-cyclones, the latter are favoured in the shallow-water approximation (and in observations).

We would like to acknowledge the useful comments of G. Flierl and D. Swift. M. Kawase first pointed out to us the analogy between an intersecting front and a PV front. E. Elliott and L. Landrum are aknowledged for comments on an early manuscript. E. B. is supported by the University of Washington Graduate School Fund and a National Science Foundation Young Investigator Award to L. T., and L. T. by the Office of Naval Research Young Investigator Award. N. P. aknowledges the support provided by the Basic Research Foundation of the Israel Academy of Sciences to the Hebrew University of Jerusalem.

Appendix A. Method of solution

The method of solution is as follows: we map the infinite domain $y = (-\infty, \infty)$ to two finite domains $U = (0, 1)$ using the mean flow as the new independent variable and using the monotonicity of the mean flow in each half of the domain (2.16):

$$U \equiv \bar{U}_1 = \begin{cases} \exp(\alpha_1 y) & \text{for } y < 0 \\ \exp(-\alpha_2 y) & \text{for } y > 0. \end{cases} \tag{A 1}$$

Thus $y = 0$ is mapped to $U = 1$ and $y = \pm\infty$ to $U = 0$. In each half of the domain the variables are expanded in Frobenius series (it is easy to show that they all have the same index γ_j):

$$\theta = \sum_{n=0}^{\infty} \theta_n U^{n+\gamma_j}, \tag{A 2}$$

where $\theta = u_1, v_1, \psi_1$ and ψ_2. Substituting this form of solution into equations (2.23)–(2.26) results in the following matrix equation for the coefficients:

$$\begin{pmatrix} -\epsilon c & -1 & 0 & 1 \\ 1 & k^2\epsilon c & 0 & \pm\alpha_j(n+\gamma_j) \\ \pm\alpha_j(n+\gamma_j) & k^2 & -Q_j & Q_j \\ 0 & 0 & F_1 & 1-\epsilon^2k^2c^2 \end{pmatrix} \begin{pmatrix} u_{1,n} \\ v_{1,n} \\ \psi_{2,n} \\ \psi_{1,n} \end{pmatrix}$$
$$= \begin{pmatrix} -\epsilon & \mp\alpha_j\epsilon & 0 & 0 \\ 0 & k^2\epsilon & 0 & 0 \\ 0 & 0 & 0 & 0 \\ 0 & 0 & F_2 & 0 \end{pmatrix} \begin{pmatrix} u_{1,n-1} \\ v_{1,n-1} \\ \psi_{2,n-1} \\ \psi_{1,n-1} \end{pmatrix}, \tag{A 3}$$

where

$$F_1 = (rQ_j - 1)\left((\gamma_j + n)^2 - k^2/Q_j\right) + \epsilon^2k^2c^2 - 1,$$
$$F_2 = \mp\alpha_j\epsilon(\gamma_j + n)(\gamma_j + n - 1) \pm k^2\epsilon/\alpha_j - 1/c,$$

and where the upper (lower) sign is used for the south, $j = 1$, (north, $j = 2$) side of the front. The variables are the same as defined in § 2 and § 3. Solving with $n = 0$ (and zero right-hand side) provides the indicial equation

$$\left(\gamma_j^2 - \frac{k^2}{Q_j}\right)\left(\gamma_j^2 - \frac{k^2}{Q_j} - \frac{rQ_j(1-\epsilon^2c^2k^2)}{(rQ_j - 1)}\right) = 0.$$

Only the roots with positive real parts belong to solutions that are well behaved at the poles. Thus, on either side of the PV front, every variable is a sum of two series.

It can be shown (taking $n \to \infty$) that for the northern ($j = 2$) series to converge at the front (where $U = 1$) $\epsilon\alpha_2 < 1$ or $\epsilon < 0.632$ (the southern series converges for all $\epsilon < \sqrt{2}$). The convergence at the front is also constrained to $rQ_j - 1 > \epsilon\alpha_j$, so that convergence becomes a problem for very shallow lower layers ($r \to 1$). In cases where the series converges at the front, we use the boundary conditions at the front and a zero-finder to solve for the phase speed c and the eigenmodes. When the series fails to converge at the front, we use the series to guide the solution out of the singularity (where $U = 0$) and shoot from there to the front. Stable and unstable modes are characterized by real and complex phase speeds, respectively.

As an additional check of the solutions we used the relation between the pseudo-energy and pseudo-momentum, $E = cM$ (see Appendix B).

Appendix B

We show here for the profile first investigated by Williams (1991) (figure 2*a*), that the pseudo-momentum cannot, in general, be used to differentiate between gravity and vortical modes. In order to do it we show that a vortical wave has a non-zero contribution from the 'gravity-wave' term in the pseudo-momentum.

Using the same notation as for the two-layer case, the linearized perturbation equations are

$$\epsilon(\bar{u}_1 - c)u_1 + (\epsilon\bar{u}_{1y} - 1)\hat{v}_1 = -\psi_1, \tag{B 1}$$
$$-k^2\epsilon(\bar{u}_1 - c)\hat{v}_1 + u_1 = -\psi_{1y}, \tag{B 2}$$
$$k^2\hat{v}_1 + u_{1y} = -Q_j\psi_1. \tag{B 3}$$

where $\hat{v}_1 \equiv v_1/ik$.

These equations can be reduced to a second-order system of ODEs with two unknowns where c is the eigenvalue. The boundary conditions are that all the perturbation amplitudes (except u_1) are continuous at $y = 0$, and that all perturbation variables vanish as $y \to \pm\infty$.

The dimensional pseudo-momentum and pseudo-energy are (Hayashi & Young 1987)

$$M = \int_{-\infty}^{\infty} \langle h_1 u_1 \rangle - \tfrac{1}{2}\overline{h}_1^2 \overline{q}_y \langle \eta^2 \rangle \mathrm{d}y, \tag{B 4}$$

and

$$E = \int_{-\infty}^{\infty} \tfrac{1}{2}\overline{h}_1(\langle u_1^2 \rangle + \langle v_1^2 \rangle) + \overline{u}_1 \langle h_1 u_1 \rangle + \tfrac{1}{2} g' \langle h_1^2 \rangle - \tfrac{1}{2}\overline{u}_1 \overline{h}_1^2 \overline{q}_y \langle \eta^2 \rangle \mathrm{d}y, \tag{B 5}$$

where angle brackets denote averages over an along-front wavelength, η is given by $(\partial_t + U\partial_x)\eta = v$ and $\overline{q}_y$ is the mean flow PV gradient. In our case $\overline{q}_y = \delta(y)\cdot(q_{12} - q_{11})$, so that the contribution of the second term in the pseudo-momentum comes from a single point ($y = 0$). The first term of the pseudo-momentum is the 'gravity-wave' contribution term according to Sakai (1988). We argued in §4 that the only mode present in Williams' profile is a vortical wave. We will show that for $\epsilon > 0$ this mode contributes to a non-zero 'gravity-wave' term of the pseudo-momentum. In addition, E and M satisfy

$$E = cM, \tag{B 6}$$

which we used as a check for the stable modes found. For unstable modes $E = M = 0$ (Hayashi & Young 1987) and the above condition is trivially satisfied.

Using the perturbation expansion derived in Williams (1991) for small ϵ ($\theta = \theta^{(0)} + \epsilon\theta^{(1)} + \ldots$) with

$$\alpha_j \equiv Q_j^{1/2}, \quad \beta_j \equiv (k^2 + Q_j)^{1/2}, \quad \gamma_j \equiv \alpha_j + \beta_j,$$

we have to first order in ϵ

$$\psi_1 = A\mathrm{e}^{-\beta_j|y|} + \epsilon 2Ak^2 \begin{cases} \dfrac{1}{\gamma_1 + \beta_1}\left[\mathrm{e}^{\gamma_1 y} - \mathrm{e}^{\beta_1 y}\right], & y < 0 \\ \dfrac{-1}{\gamma_2 + \beta_2}\left[\mathrm{e}^{-\gamma_2 y} - \mathrm{e}^{-\beta_2 y}\right], & y > 0, \end{cases}$$

$$c = 1 - \frac{\alpha_1 + \alpha_2}{\beta_1 + \beta_2} + O(\epsilon)$$

and

$$u_1 = \begin{cases} -A\beta_1 \mathrm{e}^{\beta_1 y} \\ A\beta_2 \mathrm{e}^{-\beta_2 y} \end{cases} + \epsilon A k^2 \begin{cases} \dfrac{-2}{\gamma_1 + \beta_1}\left[\gamma_1 \mathrm{e}^{\gamma_1 y} - \beta_1 \mathrm{e}^{\beta_1 y}\right] + \left(\mathrm{e}^{\alpha_1 y} - c^{(0)}\right)\mathrm{e}^{\beta_1 y}, & y < 0 \\ \dfrac{-2}{\gamma_2 + \beta_2}\left[\gamma_2 \mathrm{e}^{-\gamma_2 y} - \beta_2 \mathrm{e}^{-\beta_2 y}\right] + \left(\mathrm{e}^{\alpha_1 y} - c^{(0)}\right)\mathrm{e}^{-\beta_2 y}, & y > 0. \end{cases}$$

Using this expansion, the 'gravity-wave' term of the non-dimensional pseudo-momentum is

$$\int_{-\infty}^{\infty} \langle \psi_1 u_1 \rangle \mathrm{d}y = \epsilon A^2 k^2 \left[\frac{\alpha_1}{(\gamma_1 + \beta_1)^2} + \frac{\alpha_2}{(\gamma_2 + \beta_2)^2}\right] + O(\epsilon^2), \tag{B 7}$$

which has a positive, non-zero $O(\epsilon)$ term.

Since this integral is always zero for QG flows, Sakai (1988) interpreted it as being the gravity wave contribution to the pseudo-momentum. Here we proved that it can be non-zero for a shallow-water vortical wave.

The reason why Sakai (1988) was able to use the pseudo-momentum to distinguish between the gravity and vortical modes is that the PV distribution (and thus the mean-flow geometry) was the same in both his model and its QG limit. Here, however, the PV within the layers changes with ϵ (figure 2), making the structure of the vortical wave in the shallow-water model different from its QG limit.

REFERENCES

BARTH, J. A. 1989 Stability of a coastal upwelling front 2. Model results and comparison with observations. *J. Geophys. Res.* **94**, 10857–10883.

BARTH, J. A. 1994 Short-wavelength instabilities on coastal jets and fronts. *J. Geophys. Res.* **99**, 16095–16115.

BRETHERTON, F. P. 1966*a* Critical layer instability in baroclinic flows. *Q. J. R. Met. Soc.* **22**, 325–334.

BRETHERTON, F. P. 1966*b* Baroclinic instability and the short wavelength cut-off in terms of potential vorticity. *Q. J. R. Met. Soc.* **22**, 335–345.

FORD, R. 1993 Gravity wave generation by vortical flows in a rotating frame. PhD thesis, University of Cambridge.

GRIFFITHS, R. W., KILLWORTH, P. D. & STERN, M. E. 1982 Ageostrophic instability of ocean currents. *J. Fluid Mech.* **117**, 343–377 (referred to herein as GKS).

GRIFFITHS, R. W. & LINDEN, P. F. 1982 Laboratory experiments on fronts. *Geophys. Astrophys. Fluid Dyn.* **19**, 159–187.

HALL, M. M. & FOFONOFF, N. P. 1993 Downstream development of the Gulf Stream from 68 degrees to 55 degrees W. *J. Phys. Oceanogr.* **23**, 225–249.

HAYASHI, Y. Y. & YOUNG, W. R. 1987 Stable and unstable shear modes of rotating parallel flows in shallow water. *J. Fluid Mech.* **184**, 477–504.

KAMKE, E. 1951 *Differentialgleichungen Lösungsmethoden und Lösungen.* Akademische Verlagsgesellschaft.

KILLWORTH, P. D. 1983 Long-wave instability of an isolated front. *Geophys. Astrophys. Fluid Dyn.* **25**, 235–258.

KILLWORTH, P. D., PALDOR, N. & STERN, M. E. 1984 Wave propagation and growth on a surface front in a two-layer geostrophic current. *J. Mar. Res.* **42**, 761–785 (referred to herein as KPS).

MEACHAM, S. P. 1991 Meander evolution on piecewise-uniform, quasi-geostrophic jets. *J. Phys. Oceanogr.* **21**, 1139–1170.

NAKAMURA, N. 1988 The scale selection of baroclinic instability - effect of stratification and non-geostrophy. *J. Atmos. Sci.* **45**, 3253–3267.

NAKAMURA, N. 1993 An illustrative model of instabilities in meridionally and vertically sheared flows. *J. Atmos. Sci.* **50**, 357–375.

PALDOR, N. 1983 Linear stability and stable modes of geostrophic fronts. *Geophys. Astrophys. Fluid Dyn.* **24**, 299–326.

PALDOR, N. & GHIL, M. 1991 Shortwave instabilities of coastal currents. *Geophys. Astrophys. Fluid Dyn.* **58**, 225–241.

PEDLOSKY, J. 1987 *Geophysical Fluid Dynamics.* Springer.

PRATT, L. J. & STERN, M. E. 1986 Dynamics of potential vorticity fronts and eddy detachment. *J. Phys. Oceanogr.* **16**, 1101–1120.

RIPA, P. 1983 General stability conditions for zonal flows in a one-layer model on the β-plane or the sphere. *J. Fluid Mech.* **126**, 463–489.

SAKAI, S. 1988 Rossby-Kelvin instability: a new type of ageostrophic instability caused by a resonance between Rossby waves and gravity waves. *J. Fluid Mech.* **202**, 149–176.

STONE, P. 1970 On non-geostrophic baroclinic stability: part II. *J. Atmos. Sci.* **27**, 721–726.

SWATERS, G. E. 1991 On the baroclinic instability of cold-core coupled density fronts on a sloping continental shelf. *J. Fluid Mech.* **224**, 361–382.

TRACEY , K. L. & WATTS, D. R. 1986 On Gulf stream meander characteristics near Cape Hatteras. *J. Geophys. Res.* **91**, 7587–7602.

WATTS, D. R. & JOHNS, W. E. 1982 Gulf stream meanders: Observations on propagation and growth. *J. Geophys. Res.* **87**, 9467–9476.

WILLIAMS, R. 1991 Primitive equation models of Gulf stream meanders. *Woods Hole Ocean. Inst. Tech. Rep.* WHOI-92-16, pp. 272–285.